IAA-AAS-DyCoSS2-14-12-05

CLOSED-FORM ANALYTICAL SOLUTION BASED FEASIBLE TRAJECTORY GENERATION FOR HYPERSONIC RE-ENTRY GUIDANCE

Weiwei Cai,[*] Leping Yang,[†] Yanwei Zhu,[‡] and Yuanwen Zhang[§]

The hypersonic re-entry guidance problem is investigated in this paper with the focus on the feasible trajectory generation using path constraints control strategy. Based on the analysis of the mathematic properties of path constraints, a unified formulation describing the corresponding altitude-velocity relationship for constant path constraints is derived. Also the closed-form analytical bank angle solution is developed and compared with the one obtained from the well-known quasi-equilibrium gliding condition. Dividing the trajectory into several phases of constant path constraints, the longitudinal trajectory is rapidly planned by a search of fewer parameters. The re-entry guidance scheme is then developed using feedback linearization tracking and bank reversal strategy. Numerical simulations show that the approach proposed here steers a typical vehicle along a feasible re-entry trajectory, which satisfies both terminal and path constraints.

INTRODUCTION

To reduce cost and increase safety for space access, the second-generation reusable launch vehicles (RLVs) with a medium or high lift-to-drag aerodynamic configuration are proposed along with the development of space exploitation and utilization. Atmospheric reentry is the most critical phase for the entire mission of RLVs, and the guidance algorithm plays an important role in steering the vehicles safely while meeting the mission requirements. Moreover, the vehicles must observe strict path constraints like heating rate, aerodynamic load, dynamic pressure for structural integrity and thermal protection.[1]

Various researches have addressed the problem of hypersonic atmospheric re-entry guidance with different algorithms that can be classified into two general categories: nominal trajectory based guidance and prediction capability based guidance.[2-6] The predictor-corrector reentry guidance algorithm utilizes the time-consuming numerical integrating technique to propagate the trajectory states, and the method itself lacks efficient ways to enforce the path constraints. The nominal trajectory based guidance is believed to be more effective for the current space transportation system. Usually the nominal trajectory parameters are predesigned and stored for onboard tracking. The space shuttle like guidance algorithm provides an argument for conventional ones,

[*] PhD Candidate, National University of Defense Technology, taiweiwei@hotmail.com.
[†] Professor, National University of Defense Technology, ylp_1964@163.com .
[‡] Associate Professor, National University of Defense Technology, z9812030@hotmail.com.
[§] Lecturer, National University of Defense Technology, pointmaker8384@126.com.

and this drag acceleration profile based method has become the baseline approach for many hypersonic re-entry vehicles.[7]

Note that the selection of the approaches to enforce the aforementioned inequality path constraints directly affects the complexity of the re-entry guidance algorithms. The well-known quasi-equilibrium gliding condition (QEGC) provides an effective alternative to transform the path constraints to control inputs' limitation.[8] However, the zero flight path angle assumption of QEGC is only available in specific flight phases. The path constraint control (PCC) strategy is another choice to enforce the path constraints. Based on the normal acceleration dynamic equilibrium strategy, Xiao attempted to reduce the normal acceleration peak value by adjusting the angular rate of the attack angle.[9] In Zimmerman's research, the re-entry trajectory was divided into two phases, with the first one along a constant heating rate trajectory while the second one unconstrained.[10] Li argued the idea of constant path constraint flight, and simplified the trajectory planning into a parameters searching problem, yet only aiming at the longitudinal trajectory planning.[11] In this paper, we propose a unified formulation to describe the altitude-velocity relationship for constant path constraints, and develop the corresponding closed-form analytical bank angle solution. Using this common formulation, a path constraint control strategy based 3-DOF re-entry guidance scheme is developed.

The remainder of this paper is organized as follows. Firstly, the mathematical properties of the path constraints are analyzed and the closed-form analytical solution for the bank angle is developed. Then a comparison with the QEGC-based path constraints enforcement is conducted. Secondly, the longitudinal trajectory planning approach is investigated. The corresponding altitude-velocity profile is divided into three phases: the initial descent phase, PCC phase and check phase. By searching the parameters of the PCC phase, the nominal profile is designed satisfying the range requirements. Thirdly, the 3-DOF re-entry trajectory is generated by tracking the longitudinal trajectory through the feedback linearization technique, while the lateral motion is controlled under the bank reversal strategy. Finally, numerical simulations are presented to validate the performance of the proposed re-entry trajectory generation approach. Some useful conclusions are put forward in the end.

PROBLEM FORMULATION

Reentry Dynamics

The nondimensional equations of motion for a hypersonic re-entry vehicle over a spherical, rotating Earth are[12]:

$$
\begin{cases}
\dfrac{dz}{d\tau} = u\sin\gamma \\
\dfrac{d\theta}{d\tau} = \dfrac{u\cos\gamma\sin\psi}{z\cos\varphi} \\
\dfrac{d\varphi}{d\tau} = \dfrac{u\cos\gamma\cos\psi}{z} \\
\dfrac{du}{d\tau} = -\bar{D} - \dfrac{\sin\gamma}{z^2} + \Omega^2 z\cos\varphi(\sin\gamma\cos\varphi - \cos\gamma\sin\varphi\cos\psi) \\
\dfrac{d\gamma}{d\tau} = \dfrac{1}{u}\left[\bar{L}\cos\sigma + \dfrac{\cos\gamma}{z}\left(u^2 - \dfrac{1}{z}\right) + 2\Omega u\cos\varphi\sin\psi + \Omega^2 z\cos\varphi(\cos\gamma\cos\varphi + \sin\gamma\cos\psi\sin\varphi)\right] \\
\dfrac{d\psi}{d\tau} = \dfrac{1}{u}\left[\dfrac{\bar{L}\sin\sigma}{\cos\gamma} + \dfrac{u^2}{z}\cos\gamma\sin\psi\tan\varphi - 2\Omega u(\tan\gamma\cos\varphi\cos\psi - \sin\varphi) + \dfrac{\Omega^2 z}{\cos\gamma}\sin\varphi\cos\varphi\sin\psi\right]
\end{cases}
\tag{1}
$$

where z, u and τ are the radial distance from the center of Earth to the vehicle, the Earth-relative velocity and dimensionless time, normalized by R_0, $\sqrt{g_0 R_0}$ and $\sqrt{R_0 / g_0}$ respectively. R_0 denotes the Earth's radius at the equator and g_0 the gravity acceleration at the surface of the Earth. θ and φ are longitude and latitude, γ represents flight path angle and ψ the velocity azimuth angle. The normalized aerodynamic accelerations of lift $\bar{L}$ and drag $\bar{D}$ are given by:

$$\begin{cases} \bar{L} = \rho u^2 R_0 S_{ref} C_L / (2m) \\ \bar{D} = \rho u^2 R_0 S_{ref} C_D / (2m) \end{cases} \tag{2}$$

where ρ is the atmospheric density modeled as a simple exponential function in Eq. (3), m and S_{ref} are the vehicle mass and reference area. C_L and C_D denote the coefficients of lift and drag, which are often assumed independent of Mach number for hypersonic flying.[12]

$$\rho = \rho_0 e^{-H / H_{scale}} \tag{3}$$

where ρ_0 is the density at sea level while H_{scale} is a constant.

Define the normalized lift coefficient λ as:

$$\lambda = C_L / C_L^* \tag{4}$$

then C_L and C_D can be written as

$$\begin{cases} C_L = \lambda C_L^* \\ C_D = C_L^* \left(1 + \lambda^2\right) / (2E^*) \end{cases} \tag{5}$$

where constant E^* is the maximum lift-to-drag ratio, and C_L^* is the coefficient of lift corresponding to E^*.

Constraints

To avoid compromising the vehicle's structure and material on the great challenges induced by active aerodynamic control and increased heat load, some operational path constraints on the heating rate $\dot{Q}$, aerodynamic load n and dynamic pressure q should be considered during the hypersonic endoatmospheric flight:

$$\dot{Q} = K_{\dot{Q}} \rho^{0.5} \left(u V_c\right)^{3.15} \le \dot{Q}_{\max} \tag{6}$$

$$n = \sqrt{\bar{L}^2 + \bar{D}^2} \le n_{\max} \tag{7}$$

$$q = 0.5 \rho \left(u V_c\right)^2 \le q_{\max} \tag{8}$$

where $V_c = \sqrt{g_0 R_0}$, $K_{\dot{Q}}$ is a vehicle-specific constant, $\dot{Q}_{\max}$, $n_{\max}$ and $q_{\max}$ are the maximum values of the heating rate, aerodynamic load and dynamic pressure respectively.

Usually the control inputs of a practical system are restricted to a certain range, thus the constraints on normalized lift coefficient λ and bank angle σ are expressed as

$$\begin{cases} \lambda_{\min} \le \lambda \le \lambda_{\max} \\ \sigma_{\min} \le \sigma \le \sigma_{\max} \end{cases} \tag{9}$$

CLOSED-FORM ANALYTICAL BANK ANGLESOLUTION

Mathematical Properties of Path Constraints

In the altitude-vehicle (H-V) entry corridor, the lower boundary expressions associated with the maximum path constraints can be obtained by substituting the exponential atmospheric model Eq. (3) into Eqs. (6)~(8):

$$H=H_{scale}\ln\left(\rho_0 K_{\dot{Q}}^2\left(uV_c\right)^{6.3}/\dot{Q}^2\right) \tag{10}$$

$$H=H_{scale}\ln\left(\rho_0 u^2 R_0 g_0/(2q)\right) \tag{11}$$

$$H=H_{scale}\ln\left(\rho_0 u^2 R_0 S_{ref}\sqrt{C_L^2+C_D^2}/(2nm)\right) \tag{12}$$

Given a constant heating rate $\dot{Q}_{con}$, the relationship between variables z and u can be derived by substituting $H=R_0(z-1)$ into Eq. (10) as:

$$\begin{cases} z=(H_{scale}/R_0)\ln\left(\rho_0 K_{\dot{Q}}^2\left(uV_c\right)^{6.3}/\dot{Q}_{con}^2\right)+1\equiv(6.3H_{scale}/R_0)\ln u+C_Q \\ C_Q\equiv(H_{scale}/R_0)\ln\left(\rho_0 K_{\dot{Q}}^2 V_c^{6.3}/\dot{Q}_{con}^2\right)+1 \end{cases} \tag{13}$$

where C_Q is obviously a constant. Thus when the variables z and u satisfy Eq. (13), the heating rate would keep a constant value of $\dot{Q}_{con}$ during the re-entry flight.

Likewise, the dimensionless radial distance and velocity relationship for a given constant dynamic pressure q_{con} and aerodynamic load n_{con} can be written as:

$$\begin{cases} z=(H_{scale}/R_0)\ln\left(u^2\rho_0 R_0 g_0/(2q_{con})\right)+1\equiv(2H_{scale}/R_0)\ln u+C_q \\ C_q=(H_{scale}/R_0)\ln\left(u^2\rho_0 R_0 g_0/(2q_{con})\right)+1 \end{cases} \tag{14}$$

$$\begin{cases} z=(H_{scale}/R_0)\ln\left(\rho_0 u^2 R_0 S_{ref}\sqrt{C_L^2+C_D^2}/(2n_{con}m)\right)+1\equiv(2H_{scale}/R_0)\ln u+C_n \\ C_n=(H_{scale}/R_0)\left(\ln\left(\rho_0 R_0 S_{ref}/(2n_{con}m)\right)+\ln\left(\sqrt{C_L^2+C_D^2}\right)\right)+1 \end{cases} \tag{15}$$

The normalized lift coefficient λ varies slightly as the velocity changes during the re-entry flight, so that the second term of C_n is relatively smaller than the first one, and the parameter C_n is also taken as a constant in this research.

Since Eqs. (13)~(15) have the same format, we can easily propose a unified formulation for constant path constraints as:

$$z=k\ln u+C \tag{16}$$

where k and C take corresponding values for the heating rate, dynamic pressure and aerodynamic load respectively. It should be noted that the values of parameters k are the same for dynamic pressure and aerodynamic load, thus the z-u profiles for these two constraints are parallel, which means only one of them works. The parameter C_q is assumed to be less than C_n in this paper, and then the corresponding z-u profile consists of two phases:

$$\begin{cases} z=\left(6.3H_{scale}/R_0\right)\ln u+C_{\dot{Q}} \\ z=\left(2H_{scale}/R_0\right)\ln u+C_n \end{cases} \tag{17}$$

The dimensionless hand-off velocity can be written as:

$$u = e^{\frac{R_0(C_n - C_Q)}{4.3H_{scale}}} \tag{18}$$

Based on the aforementioned unified formulation, the closed-form analytical bank angle solution for constant path constraints can be derived as follows.

Differentiating Eq. (16) with respect to dimensionless velocity u gives:

$$\frac{dz}{du} = \frac{k}{u} \tag{19}$$

According to the 3-DOF re-entry dynamics, we can also get:

$$\frac{dz}{du} = \frac{u\sin\gamma}{-\bar{D} - \sin\gamma / z^2} \tag{20}$$

Substituting Eq. (19) into Eq. (20), the flight path angle γ can be solved:

$$\gamma = \operatorname{asin}\left(-\frac{k\bar{D}}{u^2 + k/z^2}\right) \tag{21}$$

Differentiating Eq. (21) with respect to τ yields:

$$\frac{d\gamma}{d\tau} = \frac{k}{\sqrt{\left(u^2 + k/z^2\right)^2 - \bar{D}^2k^2}}\left[-\frac{d\bar{D}}{d\tau} + \frac{\bar{D}}{u^2 + k/z^2}\frac{d}{d\tau}\left(u^2 + k/z^2\right)\right] \tag{22}$$

where the derivation of C_D with respect to variable u is ignored since the normalized lift coefficient λ varies slightly as the velocity changes.

Differentiating the dimensionless drag $\bar{D}$ with respect to τ gives:

$$\frac{d\bar{D}}{d\tau} = K\bar{D}\left[-2\rho u C_D + \frac{1}{u^2 + k/z^2}\left(\frac{R_0\rho k u^3 C_D}{H_{scale}} + \frac{2\rho k u C_D}{z^2}\right)\right] \tag{23}$$

where $K = R_0 S_{ref} / (2m)$ is a constant.

Also the last derivation term in Eq. (22) can be written as:

$$\frac{d}{d\tau}\left(u^2 + k/z^2\right) = -2\bar{D}u + \frac{2\bar{D}uk(z+k)}{z^3\left(u^2 + k/z^2\right)} \tag{24}$$

Since the altitude during the re-entry flight is much smaller than the Earth's radius, the approximation $z \approx 1$ is assumed here. Substituting Eqs. (23)~(24) into Eq. (22) yields:

$$\begin{aligned}\dot{\gamma} = \frac{kK\bar{D}}{\sqrt{\left(u^2 + k\right)^2 - \bar{D}^2k^2}}\Bigg[&2\rho u C_D - \frac{1}{u^2 + k}\left(\frac{2\bar{D}u}{K} + \frac{k\rho u^3 R_0 C_D}{H_{scale}} + 2k\rho u C_D\right) \\ &+ \frac{1}{\left(u^2 + k\right)^2}\cdot\frac{2uk(k+1)\bar{D}}{K}\Bigg]\end{aligned} \tag{25}$$

Till now, we have obtained the analytical expressions for the flight path angle (Eq. (21)) and its changing rate (Eq. (25)).

By neglecting the Coriolis and centripetal accelerations and substituting $z \approx 1$, the fifth formulation in Eq. (1) can be further simplified as:

$$\dot{\gamma} = \frac{1}{u}\left[\bar{L}\cos\sigma + \left(u^2 - 1\right)\cos\gamma\right] \tag{26}$$

Denoting Eq. (21) and (25) as $\gamma = F_2(z,u)$ and $\dot{\gamma} = F_1(z,u)$ respectively, and substituting them into Eq. (26), the closed-form analytical bank angle solution is given as:

$$\sigma = \arccos\left[\frac{uF_1(z,u) - (u^2 - 1)\cos(F_2(z,u))}{\bar{L}}\right] \tag{27}$$

If the vehicle flies a trajectory with constant path constraints, the corresponding *z*-*u* profile can be represented by Eq. (16), and the closed-form bank angle solution can be easily obtained from Eq. (27).

Comparison with QEGC

In many researches, the well-known QEGC is usually utilized to transform the path constraints to control input limitations. The QEGC assumes that the vertical acceleration component and the flight path angle are very small during the hypersonic glide flight, thus allowing the flight path angle's changing rate to be approximated as zero.[13] This reduces the fifth formulation in re-entry dynamics Eq. (1) to an algebraic equation:

$$\frac{1}{z}\left(\frac{1}{z} - u^2\right) - \bar{L}\cos\sigma = 0 \tag{28}$$

In the trajectory planning process, the relationship between normalized lift coefficient and velocity is usually predesigned, thus the variable $\bar{L}$ is determined for given velocity and there are only three dependent variables z, u and σ in Eq. (28). Thus the bank angle for a given z and u can be easily solved. Here a simple simulation is taken to compare the bank angle solutions with the aforementioned path constraints enforcement approaches.

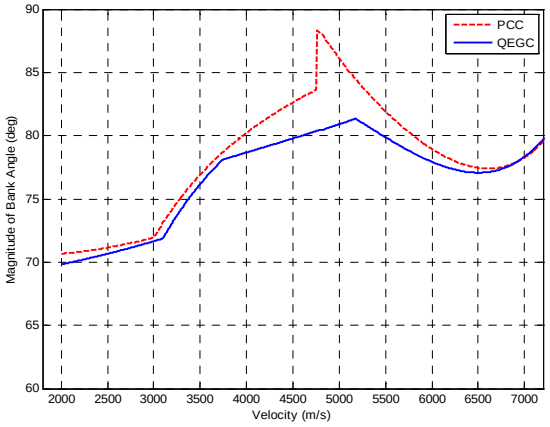

Figure 1. Comparison of Bank Angle Solution.

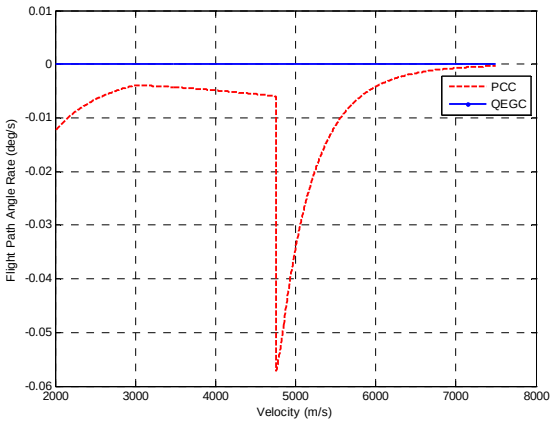

Figure 2. Changing Rate of Flight Path Angle.

The results are illustrated in Figure 1, where the solid and dashed lines describe the solutions obtained using QEGC and path constraint control (PCC) strategy respectively. In the velocity domain where path constraints work, the PCC solution is obviously larger than QEGC solution. This is mainly due to the assumption of zero path angle change rate which is the basis of QEGC.

The corresponding path angle changing rate histories are presented in Figure 2. It can be seen the path angle changing rate of PCC strategy is always negative, indicating that the QEGC seems to be much more conservative than PCC strategy. In addition, it should be noted that the PCC based bank angle solution changes greatly at the velocity of 4755 *m/s*, which is the hand-off point of heating rate constraint and dynamic pressure constraint. This phenomenon is induced by the skip of parameter *k* for different path constraints.

FEASIBLE RE-ENTRY TRAJECTORY GENERATION

Longitudinal Profile Planning

Since the trajectory associated with constant path constraints has some unified properties in the *z*-*u* profile, the longitudinal trajectory is planned in this profile and divided into three phases: the initial descent phase, PCC phase and check phase. In the initial descent phase, the atmospheric density is too low and the path constraints are not a concern, thus constant bank angle strategy is adopted. The PCC phase, the main part of entry trajectory, includes a constant heating rate segment and a constant dynamic pressure or a constant aerodynamic load segment. By adjusting the parameter of this phase, the flight range requirement will be satisfied. The check phase is designed to meet the terminal requirements of altitude, velocity or path angle.

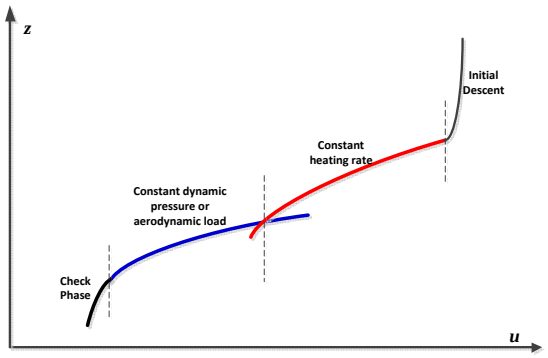

Figure 3. Composition of entry trajectory.

(1) Initial Descent Phase

Starting at the entry interface, the re-entry vehicle needs to descend and transit smoothly onto the constant heating rate profile. The initial descent trajectory is obtained by integrating the re-entry dynamics Eq. (1) numerically with given entry conditions, nominal λ and a constant bank angle. The sign of bank angle is determined by the heading error to the target. For a given constant bank angle, the reentry dynamics are integrated until the hand-off condition in Eq. (29) is satisfied.

$$\left| \frac{dz}{du} - \left(\frac{dz}{du} \right)_{heat} \right| < \delta_0 \tag{29}$$

where $\delta_0 > 0$ is a preselected value, and $(dz/du)_{heat}$ refers to the slope of the constant heating rate profile at the current point (*z, u*). If the current bank angle couldn't satisfy the requirements, its magnitude would be increased by a fixed increment repeatedly. The integrated state history, bank angle are both stored as a part of the final reference trajectory. The range-to-target at the hand-off point is also calculated and stored for later use.

(2) PCC Phase

The entry trajectory for the PCC phase can be designed as a combination of Eq. (30) and Eq. (31):

$$z = k_1 \ln u + C_1 \tag{30}$$

$$z = k_2 \ln u + C_2 \tag{31}$$

where k_1 takes the value of $6.3H_{scale}/R_0$ for the constant heating rate segment, and $k_2 = 2H_{scale} / R_0$ for the constant aerodynamic load or dynamic pressure segment. Suppose the aerodynamic load constraint works here, the values of C_1 and C_2 should satisfy:

$$\begin{cases} C_1 \geq C_{\dot{Q}} \\ C_2 \geq C_n \end{cases} \tag{32}$$

where $C_{\dot{Q}}$ and C_n are the constants for the maximum heating rate and aerodynamic load constraint.

The flight range s along an Eq. (16) like z-u profile is:

$$s = -\int \frac{zu\cos\gamma}{z^2\bar{D} + \sin\gamma} du \tag{33}$$

where the flight path angle γ can be computed with Eq. (21). The normalized aerodynamic drag $\bar{D}$ is also a function of radius and velocity, thus the flight range requirement can be satisfied by varying the z-u profile. The longitudinal trajectory planning problem is converted to the search of constants C_1 and C_2. Since the flight range is monotonic with respect to C_1 and C_2, the searching effect can be promised.

(3) Check Phase

A quadratic curve is utilized to design the entry trajectory for the check phase:

$$z = au^2 + bu + c \tag{34}$$

where the coefficients a, b and c can be determined by the terminal point (u_f, z_f), hand-off point (u_c, z_c) and the slop at the hand-off point dz_c/du_c. If there are more terminal requirements such as bank angle magnitude, a higher-order curve function would be a better alternative.

Similar to the aforementioned closed-form analytical bank angle solution, the path angle and its changing rate associated with Eq. (34) can be written as:

$$\gamma = \operatorname{asin}\left(\frac{-W\bar{D}}{u + W/z^2}\right) \tag{35}$$

$$\dot{\gamma} = -\frac{1}{\sqrt{(u+W)^2 - (W\bar{D})^2}}\left[(\dot{W}\bar{D} + W\dot{\bar{D}}) - \frac{W\bar{D}}{u+W}\left(\dot{u} + \dot{W} - 2uW\sin\gamma\right)\right] \tag{36}$$

where $W = 2au + b$, $\dot{W} = 2a\dot{u}$.

Substituting Eqs. (35)~ (36) into Eq. (27) yields the corresponding bank angle solution for the check phase.

3-DOF Trajectory Generation

When the preceding three parts of planning process are completed, the longitudinal profile is obtained for the entire entry trajectory, but not a correct lateral profile. Moreover, the longitudinal

trajectory planning process has ignored the Earth's rotating terms in the re-entry dynamics. To generate the 3-DOF re-entry trajectory, the predesigned longitudinal profile is tracked by the feedback linearization technique, and the sign of bank angle is determined by the heading error strategy.

The second-order derivative of variable z is:

$$\begin{aligned} \ddot{z} &= (-\bar{D}\sin\gamma + \frac{u^2\cos\gamma}{z} - \frac{1}{z^2}) + \nu\cos\gamma \\ &\equiv a(x) + b(x)\nu \end{aligned} \tag{37}$$

where $\nu = \bar{L}\cos\sigma$ and $b(x) \neq 0$ during the re-entry flight. The state feedback control law is given by:

$$\nu = (w - a(x)) / b(x) \tag{38}$$

where w is the equivalent control input. Substituting Eq. (38) into Eq. (37) yields:

$$\ddot{z} = w \tag{39}$$

The reference longitudinal profile tracking error and its derivatives are defined as:

$$\begin{cases} e = z - z_{ref} \\ \dot{e} = \dot{z} - \dot{z}_{ref} \\ \ddot{e} = w - \ddot{z}_{ref} \end{cases} \tag{40}$$

To formulte closed-loop error dynamics in the linear time-invariant form, the tracking error dynamics are modeled as a second-order system:

$$\ddot{e} + 2\varsigma\omega\dot{e} + \omega^2 e = 0 \tag{41}$$

where $\varsigma > 0$ is the damping coefficient, and $\omega > 0$ denotes the natural frequency. According to Eq. (41), the equivalent control input is given by:

$$w = \ddot{z}_{ref} - 2\varsigma\omega\dot{e} - \omega^2 e \tag{42}$$

Substituting Eq. (42) into Eq. (38), and combining with the definition of ν, the bank angle can be written as:

$$\sigma = \text{acos}\left(\frac{\ddot{z}_{ref} - 2\varsigma\omega\dot{e} - \omega^2 e - a(x)}{\bar{L}b(x)} \right) \tag{43}$$

The lateral motion is controlled by changing the sign of bank angle repeatedly according to the flight heading angle error corridor. Here the heading angle error is defined as the error between the velocity heading angle and the line-of-sight (LOS) angle with respect to target. The LOS angle can be computed by Eq. (44):

$$\tan\psi_{LOS} = \frac{\sin(\theta_T - \theta)}{\cos\varphi\tan\varphi_T - \sin\varphi\cos(\theta_T - \theta)} \tag{44}$$

where (θ, φ) is the current position of the re-entry vehicle while (θ_T, φ_T) is the target's position.

The heading error corridor is designed as a piecewise function of velocity. If the heading angle error stays in the error corridor, the sign of bank angle keeps unchanged; however, when the heading error is beyond the corridor's boundaries, a sign reversal operation takes place.[14] The symbol description for the reversal logic is:

$$\operatorname{sign}\left(\sigma^{i}\left(u\right)\right)=\begin{cases}-1 & \Delta\psi \geq \Delta\psi_{Bund} \\ 1 & \Delta\psi \leq -\Delta\psi_{Bund} \\ \operatorname{sign}\left(\sigma^{i-1}\left(u\right)\right) & -\Delta\psi_{Bund} < \Delta\psi < \Delta\psi_{Bund}\end{cases} \tag{45}$$

where $\operatorname{sign}(\sigma^{i-1}(u))$ denotes the sign of bank angle in the last sample period.

With the longitudinal profile tracking and bank angle reversal, the control inputs for re-entry flight have been determined, and the 3-DOF trajectory can be obtained by integrating the re-entry dynamics in Eq. (1).

NUMERICAL SIMULATIONS

In this section, we present the simulation results of 3-DOF trajectory generation using the PCC approach investigated here. The re-entry vehicle's aerodynamics and physical parameters are based on the CAV-H data.[15] A time history of angle of attack like space shuttle is utilized and the re-entry mission description is presented in Table 1.

Table 1. Re-entry Mission Description.

Constraints	Values
Boundary Constraints	Initial: $h_0 = 90\ km$, $\theta_0 = 0°$, $\varphi_0 = 0°$, $v_0 = 7500\ m/s$, $\gamma_0 = 0$, $\psi_0 = 79^\circ$
	Terminal: $h_f = 30km$, $\theta_f = 90^\circ$, $\varphi_f = 15°$, $v_f = 2500m/s$
Path Constraints	$\lambda \in [0, 2]$, $\sigma \in [-80^\circ, 80^\circ]$
	$n_{\max}$=4g, $q_{\max}$=110 kPa, $\dot{Q}_{\max}$ =1700 kw/m^2

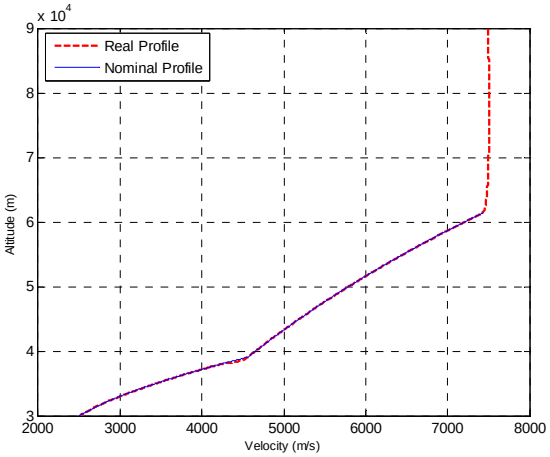

Figure 4. Longitudinal Profile.

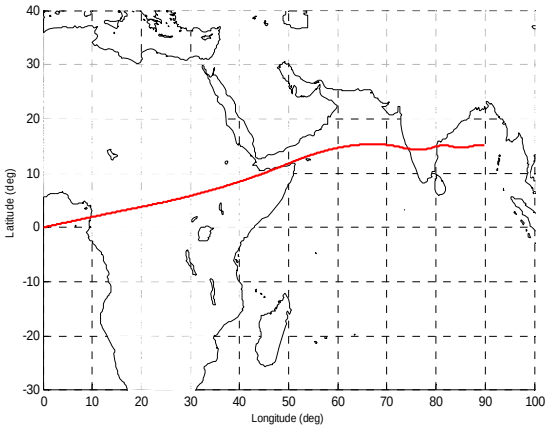

Figure 5. Longitude-Latitude Curve.

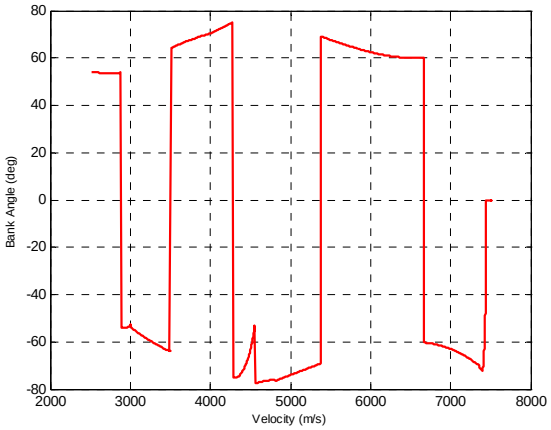

Figure 6. Bank Angle.

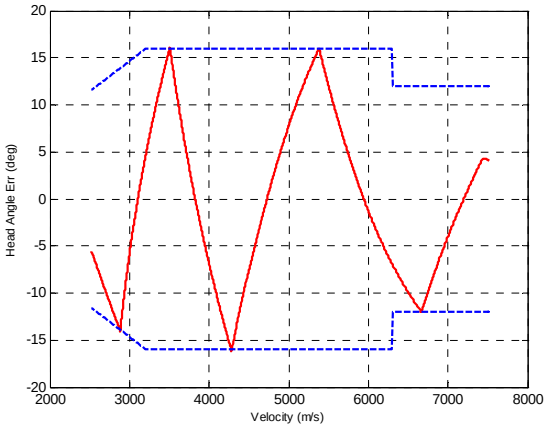

Figure 7. Heading Angle Error.

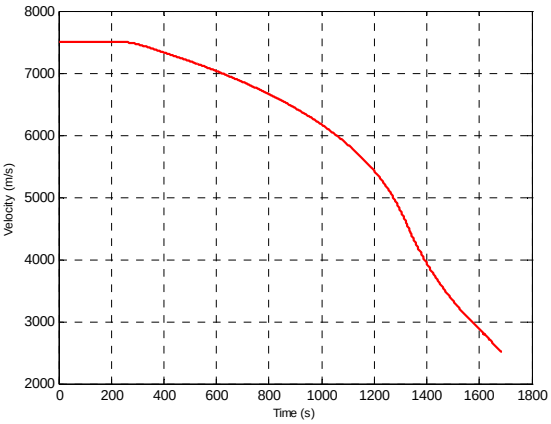

Figure 8. Time history of Velocity.

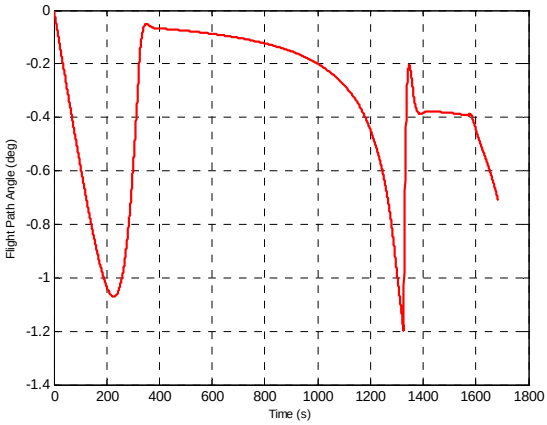

Figure 9. Time history of Flight Path Angle.

Since the initial descent trajectory is obtained by integrating the 3-DOF re-entry dynamics with a constant bank angle, only the PCC and check trajectories are tracked in the simulation. As shown in Figure 4, the tracking error of the nominal longitudinal profile is very small, verifying the validity of the feedback linearization tracking technique. Figure 5 presents the history of the re-entry vehicle's position. Due to the lateral control strategy, the vehicle would swing around the target plane in the real flight, resulting in a terminal range error of 18.073*km*. To improve the terminal position precision, some flight range updating techniques can be introduced, which would be investigated in the future. Enforced by the heading error corridor, the sign of bank angle has reversed five times, and the heading error has been controlled in the corridor. The time history of velocity is presented in Figure 8. The terminal velocity error is 17.84 *m/s*, satisfying the requirement. According to the time history of path angle in Figure 9, the flight path angle is small and negative for the entire mission. As mentioned above, the path angle changes greatly around the velocity of 4600 *m/s*, which is the hand-off point of the constant heating rate and aerodynamic load phases.

CONCLUSION

Concentrating on the hypersonic re-entry guidance problem, this paper presents a study of feasible trajectory generation approach using path constraint control strategy. Some useful conclusions are drawn as follows. Firstly, for constant path constraints, the re-entry trajectory in *z-u* profile can be expressed with a unified formulation, and the corresponding closed-form analytical bank-angle solution is developed. Secondly, the QEGC-based path constraints enforcement approach is more conservative than the approach studied here. Thirdly, utilizing the path constraint control strategy, the longitudinal trajectory planning is realized by searching two parameters, reducing the computational burden. Numerical simulations have verified the validity of the proposed re-entry guidance scheme.

REFERENCES

1. Jorris TR, Cobb RG. Three-Dimensional Trajectory Optimization Satisfying Waypoint and No-Fly Zone Constraints. Journal of Guidance, Control, and Dynamics 2009; 32(2): 551-572.
2. Joshi A, Sivan K, Amma SS. Predictor-Corrector Reentry Guidance Algorithm with Path Constraints for Atmospheric Entry Vehicles. Journal of Guidance, Control, and Dynamics 2007; 30(5): 1307-1318.
3. Lu P. Predictor-Corrector Entry Guidance for Low-Lifting Vehicles. Journal of Guidance, Control, and Dynamics 2008; 31(4): 1067-1075.
4. Shaffer PJ, Ross IM, Oppenheimer MW, Domain DB. Optimal trajectory reconfiguration and retargeting for a reusable launch vehicle. AIAA Guidance, Navigation, and Control Conference and Exhibit 2005: 1-14.
5. Shen Z, Hu Y, Ren Z, Song J-s. A New On-line Planning Method for RLV reentry trajectory design. Journal of Astronautics 2011; 32(8): 1670-1675.
6. Morio V, Cazaurang F, Vernis P. Flatness-based Hypersonic Reentry Guidance of a Lifting-body Vehicle. Control Engineering Practice 2009; 17(5): 588-596.
7. Harpold JC, Graves CA. Shuttle Entry Guidance. 1979.
8. Shen Z, Lu P. On-board Generaation of Three-Dimensional Constrained Entry Trajectories. AIAA Guidance, Navigation, and Control Conference and Exhibit 2002.
9. Xiao X-X, Li W-H, Zhang H. Research on Attack Angle Design Method for Sub-Orbital Vehicle Re-entry to Reduce the Normal Acceleration Peak Value. Journal of Astronautics 2012; 33(1): 40-47.
10. Zimmerman C, Dukeman GA, Hanson J. Automated method to compute orbital reentry trajectories with heating constraints. Journal of Guidance, Control, and Dynamics 2003; 26(4): 523-529.
11. Li H, Zhang R, Li Z, Zhang R. New Method to Enforce Inequality Constraints of Entry Trajectories. Journal of Guidance, Control, and Dynamics 2012; 35(5): 1662-1667.
12. Vinh NX, Busemann A, Culp RD. Hypersonic and planetary entry flight mechanics. Ann Arbor: The University of Michigan Press, 1980.
13. Lu P. Asymptotic Analysis of Quasi-Equilibrium Glide in Lifting Entry Flight. Atmospheric Flight Mechanics Conference and Exhibit 2005.
14. Hu Z. Research on Trajectory planning and guidance for space-based strike weapon. Changsha: National University of Defense Technology, 2009.
15. Phillips TH. A Common Aero Vehicle (CAV) Model, Description, and Employment Guide. 2003.